BOREHOLE SEISMIC SOURCE RADIATION IN LAYERED ISOTROPIC AND ANISOTROPIC MEDIA: BOUNDARY ELEMENT MODELING

by

Wenjie Dong, Michel Bouchon, and M.N. Toksöz

Earth Resources Laboratory
Department of Earth, Atmospheric, and Planetary Sciences
Massachusetts Institute of Technology
Cambridge, MA 02139

ABSTRACT

An algorithm based on the boundary element method is established for modeling seismic source radiation from open or cased boreholes in layered transversely isotropic (TI) media. The axis of symmetry of TI layers is assumed to be parallel to the borehole axis. Under this assumption, the problem is significantly simplified because the element discretization of the borehole remains one dimensional. For fluid-filled open boreholes, three equivalent sources on each element are required to represent the boundary effects on the inner fluid and the outer solid. The three boundary conditions for a fluid-solid interface set up a system of equations for the equivalent sources on all elements. Once the sources are known, displacements in the solid and pressure in the fluid are obtained. For fluid-filled and cased boreholes, the method treats borehole fluid, casing, and cement as a cylindrically layered isotropic medium. In this case, the boundary conditions to be satisfied at the borehole wall are four (continuity of the normal and tangential displacements and stresses). The implementation of the method is illustrated through a few examples.

INTRODUCTION

Wave propagation along a fluid-filled borehole embedded in an isotropic or transversely isotropic half space has been studied by matching boundary conditions on the borehole wall and evaluating wave number integrals (Cheng and Toksöz, 1981; Schoenberg *et al.*, 1981; White and Tongtaow, 1981; Schmitt and Bouchon, 1985; Schmitt, 1989). Tubman *et al.* (1984) applied the same method for waves in a cased borehole embedded in a homogeneous isotropic half space. The radiation pattern of borehole sources in homogeneous isotropic and anisotropic media have been studied in a similar fashion (Lee and Balch, 1981; Meredith, 1990; Winbow, 1991; Gibson, 1993; Dong and Toksöz, 1993). If the formation becomes inhomogeneous, this method no longer applies and other numerical techniques have to be utilized. The finite difference and finite element methods have been extensively used by many researchers to investigate the acoustic logging problems (Stephen *et al.*, 1985; Randall *et al.*, 1991; Ellefsen, 1990). Difficulties arise when these

two methods are used to model radiation into the formation at some distance from the borehole, because of the large scale difference between borehole diameter and formation extent. The ability to calculate the solution is then severely restricted by memory space needed for both methods. Accuracy of these methods is also hampered by grid dispersion and inaccurate handling of fluid and formation interface.

A boundary element-based modeling technique proposed by Bouchon (1993) overcomes these problems. The boundary element method (BEM) is well suited to the borehole geometry and the scale problem is easily dealt with. Bouchon (1993) used the method in an infinite open borehole in layered isotropic media. Prior to this implementation, BEM was used by Kawase (1988) in studying seismic wave scattering by surface topographies. Bouchon and Schmitt (1989) applied a boundary integral and discrete wavenumber formulation to model an irregular borehole in a homogeneous formation.

This paper presents two extensions to Bouchon's BEM modeling method. First, the formation is generalized to incorporate transversely isotropic layers. This is important because many sedimentary rocks exhibit transverse isotropy (e.g., Thomsen, 1986). Including anisotropy will lead to a better understanding of real data. The other extension is to include casing and cement in the formulation. The effect of casing and cement has been shown to have significant influence on the logging waveform (Tubman *et al.*, 1984). They also strongly affect wave diffraction and radiation into the formation. Figure 1 shows the configuration of the problem. In addition to the explosion source, other source types, such as the vertical and orbital vibrators and bender source, are also accommodated. Examples are given at the end to illustrate the implementation.

THE INDIRECT BEM METHOD

There are two types of BEM implementation. The one often used by engineers is called the *direct formulation*, where both the field and its gradient are solved for (e.g., Banerjee and Rutterfield, 1981; Brebbia and Dominguez, 1989). This approach is the one usually applied in the static problems of elasticity. Another approach used in wave propagation is named *indirect formulation*, because the quantities to be solved at the boundary have no direct physical meanings. In the following, the indirect formulation is used and its implementation is discussed.

Indirect Boundary Integral Equations

If a volume point source is placed inside a fluid-filled borehole, the total displacement potential in the borehole fluid is the sum of a direct potential pertaining to the source and a reflected potential due to the boundary. In the case of steady state radiation (or in the frequency domain) the reflected field can be expressed as the integral of a fictitious source distribution over the borehole surface, with the Green's function being the integrand. Therefore, the displacement potential in the fluid is

$$\phi_1(\mathbf{x}) = \phi_i + \int_B dS' g_1(\mathbf{x}, \mathbf{x}')\psi(\mathbf{x}') \quad \text{for } \mathbf{x} \in V_b + B \ , \tag{1}$$

where, the volume of borehole fluid and the borehole surface are denoted by V_b and B respectively. Subscript 1 stands for the fluid region and ϕ_i is the incident potential. The fictitious source distribution over the borehole surface is denoted by $\psi(\mathbf{x}')$. Integral kernel, g_1, is the scalar Green's function in an infinite homogeneous medium. It may be expressed in the well-known form

$$g_1(\mathbf{x},\mathbf{x}') = \frac{e^{ik_f|\mathbf{x}-\mathbf{x}'|}}{4\pi|\mathbf{x}-\mathbf{x}'|}, \tag{2}$$

where, $k_f = \omega/c_f$ is the wavenumber for the fluid. Equation (1) states that the influence of the elastic medium on the wavefield inside the borehole is equivalent to impressing a sheet of fictitious sources on the boundary between the fluid and the elastic medium. The fictitious source distribution density is the unknown function to be determined. Figure 2 shows the equivalent problem for the borehole fluid in open and cased boreholes.

For the source-free elastic medium outside the borehole, the displacement field can be expressed as

$$\mathbf{U}_2(\mathbf{x}) = \int_B dS' \overline{\mathbf{G}}(\mathbf{x},\mathbf{x}') \cdot \Psi(\mathbf{x}') \quad \text{for } \mathbf{x} \in V_e + B, \tag{3}$$

where, $\Psi(\mathbf{x}')$ is a vector fictitious source distribution on the boundary. $\overline{\mathbf{G}}(\mathbf{x},\mathbf{x}')$ is the dyadic Green's function for displacement and has the following form for a homogeneous isotropic formation

$$\overline{\mathbf{G}}(\mathbf{x},\mathbf{x}') = \frac{1}{\rho\omega^2}\left\{k_\beta^2 \overline{\mathbf{I}} g_\beta(\mathbf{x},\mathbf{x}') + \nabla\nabla\left[g_\beta(\mathbf{x},\mathbf{x}') - g_\alpha(\mathbf{x},\mathbf{x}')\right]\right\}. \tag{4}$$

Here, g_α and g_β are scalar Green's functions of the same form as in Equation (2), except that k_f is changed to k_α for the dilatational wave and to k_β for the shear wave. Equation (3) says that the displacement in the outside region, (V_e), results from the vector fictitious source distributed along the boundary. For axially symmetrical problems in cylindrical coordinates, the vector fictitious source can be decomposed into source distributions in radial and vertical directions. Therefore, one has to determine the two unknown distribution functions before calculating the displacement field in the elastic medium. Figure 3 describes the equivalent problem for the surrounding formation.

BEM Implementation

The essence of Indirect BEM implementation is to discretize the boundary between borehole fluid and the surrounding formation into a set of small size surfaces called elements. Each element is a ring-shaped surface with height dz and borehole radius r_0. The density of the fictitious source is assumed to be constant on each element. According to the previous boundary integrals, a fictitious volume source distribution for the fluid, and a fictitious source vector for the elastic medium are required in order to uniquely describe the borehole source radiation. A fictitious source vector in an axially symmetrical system consists of the vertical and radial components only. Therefore, on each element, i, three unknowns are to be determined: the fictitious fluid volume source, V_i^f; the vertical source for the elastic medium, F_i^v; and the radial source for the

elastic medium, F_i^r. Our goal is to obtain these sources on each element so that one can calculate the displacement fields in the elastic medium and the pressure in the fluid.

The maximum number of elements is restricted by the power of current computers and the specified accuracy. In practice, three elements per shortest wavelength are used and the number of elements depends on the time window and the fastest wave speed. Thus, the element heights dz and the number of elements, N_e, are

$$dz = \frac{\min(c, \beta)}{3f}, \quad N_e = \frac{3f \times t_{max} \times \alpha}{\min(c, \beta)}. \tag{5}$$

The frequency and the maximum time window are denoted by f and t_{max}. With each element, the usual fluid/solid boundary conditions for open borehole, and the solid/solid boundary conditions for cased borehole, have to be satisfied. The boundary conditions are satisfied at the center of each element. Displacements and stresses (or pressure) at the center of each element are contributed by all three fictitious sources on all the elements. To calculate the displacement at the j-th element due to a source at the i-th element, we use the indirect formulations in Equations (1) and (3). At the j-th element, the boundary conditions for the open borehole case become

$$\begin{aligned}
\sum_{i=1}^{N_e} A_{ji}^f V_i^f + \sum_{i=1}^{N_e} A_{ji}^v F_i^v + \sum_{i=1}^{N_e} A_{ji}^r F_i^r &= D_j^u, \\
\sum_{i=1}^{N_e} B_{ji}^f V_i^f + \sum_{i=1}^{N_e} B_{ji}^v F_i^v + \sum_{i=1}^{N_e} B_{ji}^r F_i^r &= D_j^{\sigma_{rr}}, \\
\sum_{i=1}^{N_e} C_{ji}^v F_i^v + \sum_{i=1}^{N_e} C_{ji}^r F_i^r &= D_j^{\sigma_{rz}}.
\end{aligned} \tag{6}$$

A_{ji}^f, A_{ji}^v and A_{ji}^r represent displacements at the j-th element due to the volume, vertical, and radial ring sources of unit strength at the i-th element, respectively. They are surface integrals of the Green's functions over the surfaces of the borehole (bottom + wall). The B's and C's are the radial and tangential stresses at the j-th element due to sources at the i-th element. They are the surface integrals of the stress Green's function. The D's are the exciting fields or initial data (indicated by their superscripts) at the j-th element. With j ranging from 1 to N_e, we obtain $3 \times N_e$ equations that can be solved for the $3 \times N_e$ unknowns. Once these fictitious source densities are available, fields inside and outside the borehole can be easily obtained using Equations (1) and (3).

Element Surface Integration

Surface integration of Green's functions is accomplished in two steps. The integrals are first transformed into wave number integrals by applying the Sommerfeld integral representation to the function e^{ikR}/R. The wavenumber integration is then evaluated by the discrete wavenumber method.

Expressed in a horizontal wavenumber integral, the scalar Green's function, g_1, is

$$g_1 = \frac{i}{4\pi}\int_0^\infty \frac{k}{\nu_f} J_0(kD) e^{i\nu_f|z-z'|} dk, \tag{7}$$

where $\nu_f = \sqrt{k_f^2 - k^2}$ and $D = \sqrt{r^2 + r_0^2 - 2rr_0\cos(\varphi - \varphi_0)}$ is the source-receiver distance. Physically, this equation represents the synthesis of a spherical wavefront using infinitely many cylindrical wavefronts. It is the use of the Sommerfeld integral representation that allows vertical layering to be incorporated. Using the addition theorem for the zeroth order Bessel function (Watson, 1944)

$$J_0(kD) = \sum_{m=0}^{\infty} \varepsilon_m J_m(kr) J_m(kr_0) \cos m(\varphi - \varphi_0), \tag{8}$$

one obtains

$$g_1 = \frac{i}{4\pi}\sum_{m=0}^{\infty} \varepsilon_m \cos m(\varphi - \varphi_0) \int_0^\infty \frac{k}{\nu_f} J_m(kr_0) J_m(kr) e^{i\nu_f|z-z'|} dk, \tag{9}$$

where, $\varepsilon_0 = 1$ and $\varepsilon_m = 2$ for $m \geq 1$, and J_m is the m-th order Bessel function of the first kind. Given the above relations, the $r_0 d\varphi_0$ part of surface integration ($r_0 d\varphi_0 dz$) simplifies the integrand of the wavenumber integral significantly, thanks to the orthogonal cosine and sine functions over the range of 0 to 2π. *The result of this integration represents the response of a circular ring source.* The dz part of the surface integral can be analytically evaluated through integrating the ring source results over z'. Thus, the element surface integration of the Green's function basically reduces to a horizontal wavenumber integral. Essentially, this simplification results from the axial symmetry of the problem.

The coefficients in Equation (6) form a fully populated, non-symmetrical, and complex matrix. This is often regarded as the disadvantage of BEM as compared to FEM or FDM. In the latter two methods, tridiagonal matrices are obtained, and a special faster algorithm exists for this kind of matrix. Nevertheless, this matrix can still be easily manipulated as the number of elements is not exceedingly high and the system of equations is only solved once for each frequency.

RING SOURCE RESULTS IN TI MEDIA

If the surrounding formation is anisotropic with a low degree of symmetry, the Green's function cannot be reduced to a simple expression like Equation (4). However, for a transversely isotropic medium, Dong (1993) and Dong and Schmitt (1993) provided a simple and numerically feasible Green's function similar to the isotropic Green's function. The dynamic Green's function in a transversely isotropic medium is

$$\overline{\mathbf{G}} = g\bar{\mathbf{I}}_t + \hat{z}\hat{z}L_z\phi - (c_{13} + c_{44})(\nabla_t\hat{z} + \hat{z}\nabla_t)\frac{\partial\phi}{\partial z} + \nabla_t\nabla_t\psi. \tag{10}$$

The individual symbols are

$$
\begin{aligned}
L_z &= c_{11}\nabla_t^2 + c_{44}\frac{\partial^2}{\partial z^2} + \rho\omega^2, \\
g(\mathbf{x},\mathbf{x}') &= \frac{i}{4\pi c_{44}}\int_0^\infty \frac{e^{i\nu_c|z-z'|}}{\nu_c} kJ_0(kD)dk, \\
\phi(\mathbf{x},\mathbf{x}') &= \frac{-i}{4\pi c_{33}c_{44}}\int_0^\infty \frac{1}{\nu_b^2-\nu_a^2}\left(\frac{e^{i\nu_b|z-z'|}}{\nu_b} - \frac{e^{i\nu_a|z-z'|}}{\nu_a}\right) kJ_0(kD)dk, \\
\psi(\mathbf{x},\mathbf{x}') &= \frac{i}{4\pi}\int_0^\infty f(z,z')\; kJ_0(kD)dk, \\
f(z,z') &= -\frac{(c_{13}+c_{44})^2\nu_a}{c_{33}c_{44}^2(\nu_b^2-\nu_a^2)(\nu_z^2-\nu_a^2)}e^{i\nu_a|z-z'|} \\
&\quad + \frac{(c_{13}+c_{44})^2\nu_b}{c_{33}c_{44}^2(\nu_b^2-\nu_a^2)(\nu_z^2-\nu_b^2)}e^{i\nu_b|z-z'|} - \frac{c_{11}-c_{66}}{c_{44}^2\nu_c(\nu_z^2-\nu_c^2)}e^{i\nu_c|z-z'|}.
\end{aligned}
$$

In these equations, k is the horizontal wave number, $D = \sqrt{r^2 + r_0^2 - 2rr_0\cos(\varphi-\varphi_0)}$ is the source-receiver distance. The five elastic constants are c_{11}, c_{33}, c_{13}, c_{44}, and c_{66}. ν_a, ν_b, and ν_c are the vertical wave numbers for the *quasi-P*, *quasi-SV*, and *quasi-SH* waves in the medium, respectively. ν_a and ν_b are the solutions of the following equation

$$
\begin{aligned}
c_{33}c_{44}k_z^4 &+ [(c_{11}c_{33} - c_{13}^2 - 2c_{13}c_{44})k^2 - (c_{33}+c_{44})\rho\omega^2]k_z^2 \\
&+ (c_{44}k^2 - \rho\omega^2)(c_{11}k^2 - \rho\omega^2) = 0, \qquad (11)
\end{aligned}
$$

and $\nu_c = \sqrt{(\rho\omega^2 - c_{66}k^2)/c_{44}}$ and $\nu_z = \sqrt{(\rho\omega^2 - c_{11}k^2)/c_{44}}$.

Vertical Ring Forces

For a vertical ring source of unit strength, $\mathbf{F} = \hat{z}\delta(z-z')\delta(r-r_0)$. Integration over φ_0 is nonzero only for $m = 0$ according to the orthogonality of the set $\{1, \cos\varphi, \cos 2\varphi, ...\}$. The two displacement components are

$$
U_r = \frac{\mathrm{sgn}(z-z')}{2}\int_0^\infty S_{ab}k^2 r_0 J_0(kr_0)J_1(kr)\left[e^{i\nu_b|z-z'|} - e^{i\nu_a|z-z'|}\right]dk, \qquad (12)
$$

$$
U_z = \frac{i}{2}\int_0^\infty kr_0 J_0(kr_0)J_0(kr)\left[S_b e^{i\nu_b|z-z'|} - S_a e^{i\nu_a|z-z'|}\right]dk, \qquad (13)
$$

where,

$$
S_{ab} = \frac{c_{13}+c_{44}}{c_{33}c_{44}(\nu_b^2-\nu_a^2)}, \quad S_a = \frac{\nu_a^2-\nu_z^2}{c_{33}(\nu_b^2-\nu_a^2)\nu_a}, \quad S_b = \frac{\nu_b^2-\nu_z^2}{c_{33}(\nu_b^2-\nu_a^2)\nu_b}.
$$

Using U_r and U_z in the equations for strain and stresses in cylindrical coordinates, and bearing in mind that the static contribution has to be taken into account in σ_{rz} when the observation point is at the source point, we obtain the stresses at $\mathbf{x} = (r, z)$:

$$
\sigma_{rr} = \frac{\mathrm{sgn}(z-z')}{2}\int_0^\infty kr_0 J_0(kr_0)I_0 dk, \qquad (14)
$$

$$
\begin{aligned}
I_0 = \; & \left[-(c_{11}S_{ab}k^2 - c_{13}S_a\nu_a)J_0(kr) + 2c_{66}kS_{ab}J_1(kr)/r\right] e^{i\nu_a|z-z'|} \\
& + \left[(c_{11}S_{ab}k^2 - c_{13}S_b\nu_b)J_0(kr) - 2c_{66}kS_{ab}J_1(kr)/r\right] e^{i\nu_b|z-z'|}, \\
\sigma_{rz} = \; & -\frac{1}{2}\delta(z-z') + \frac{i}{2}\int_0^\infty k^2 r_0 J_0(kr_0)J_1(kr)I_1 dk, \qquad (15) \\
I_1 = \; & -c_{44}(S_{ab}\nu_a - S_a)e^{i\nu_a|z-z'|} + c_{44}(S_{ab}\nu_b - S_b)e^{i\nu_b|z-z'|} \; .
\end{aligned}
$$

Radial Ring Forces

For a radial ring source of unit strength, $\mathbf{F}(\mathbf{x}) = [\hat{r}\cos(\varphi-\varphi_0) - \hat{\varphi}\sin(\varphi-\varphi_0)]\delta(r-r_0)\delta(z-z')$. Using orthogonality in the integration over φ_0, we obtain displacements at (r,z) by a ring of radial forces at $\mathbf{x}' = (r_0, z')$ in a TI medium:

$$
\begin{aligned}
U_r &= \frac{i}{2}\int_0^\infty kr_0 J_1(kr_0)J_1(kr)\left[T_a e^{i\nu_a|z-z'|} - T_b e^{i\nu_b|z-z'|}\right] dk, \qquad (16) \\
U_z &= \frac{\mathrm{sgn}(z-z')}{2}\int_0^\infty S_{ab}k^2 r_0 J_1(kr_0)J_0(kr)\left[e^{i\nu_a|z-z'|} - e^{i\nu_b|z-z'|}\right] dk. \qquad (17)
\end{aligned}
$$

The stresses are

$$
\begin{aligned}
\sigma_{rr} = \; & -\frac{1}{2}\delta(z-z') + \frac{i}{2}\int_0^\infty kr_0 J_1(kr_0)I_3 dk, \qquad (18) \\
I_3 = \; & \left[(c_{11}T_a + c_{13}S_{ab}\nu_a)kJ_0(kr) - 2c_{66}T_a J_1(kr)/r\right] e^{i\nu_a|z-z'|} \\
& - \left[(c_{11}T_b + c_{13}S_{ab}\nu_b)kJ_0(kr) - 2c_{66}T_b J_1(kr)/r\right] e^{i\nu_b|z-z'|}, \\
\sigma_{rz} = \; & \frac{\mathrm{sgn}(z-z')}{2}\int_0^\infty kr_0 J_1(kr_0)J_1(kr)I_4 dk, \qquad (19) \\
I_4 = \; & c_{44}\left\{(T_b\nu_b + k^2 S_{ab})e^{i\nu_b|z-z'|} - (T_a\nu_a + k^2 S_{ab})e^{i\nu_a|z-z'|}\right\} \; .
\end{aligned}
$$

In the above equations,

$$
T_a = \frac{(c_{13}+c_{44})^2\nu_a k^2}{c_{33}c_{44}^2(\nu_b^2-\nu_a^2)(\nu_z^2-\nu_a^2)}, \quad T_b = \frac{(c_{13}+c_{44})^2\nu_b k^2}{c_{33}c_{44}^2(\nu_b^2-\nu_a^2)(\nu_z^2-\nu_b^2)}.
$$

Explosive Ring Source in Fluid

For a ring of explosive point sources, the displacement potential is obtained by integrating Equation (2) with respect to angle φ_0,

$$
\phi = -\frac{i}{2}\int_0^\infty \frac{kr_0}{\nu_f} J_0(kr_0)J_0(kr)e^{i\nu_f|z-z'|}dk. \qquad (20)
$$

Upon taking the derivative of this potential with respect to r and z, and adding the static contribution to U_r for a volume source, we obtain

$$
\begin{aligned}
U_r &= -\frac{1}{2}\delta(z-z') + \frac{i}{2}\int_0^\infty \frac{k^2 r_0}{\nu_f} J_0(kr_0)J_1(kr)e^{i\nu_f|z-z'|}dk, \qquad (21) \\
U_z &= \frac{\mathrm{sgn}(z-z')}{2}\int_0^\infty kr_0 J_0(kr_0)J_0(kr)e^{i\nu_f|z-z'|}dk. \qquad (22)
\end{aligned}
$$

The stresses inside the fluid are

$$\sigma_{rr} = \frac{i}{2\rho\omega^2}\int_0^\infty \frac{kr_0}{\nu_f} J_0(kr_0)J_0(kr)e^{i\nu_f|z-z'|}dk, \tag{23}$$

$$\sigma_{rz} = 0. \tag{24}$$

INCORPORATION OF LAYERED TI FORMATION

From the displacement and stress expressions for the circular sources, we may infer that for a given k (plane wave), the recorded displacements and stresses at a receiver away from the circular source in a layered TI medium would have the following form:

$$\begin{array}{ll} U_r(r,z) = \int_0^\infty u_r(k,z)\, kJ_1(kr)dk, & U_z(r,z) = \int_0^\infty u_z(k,z)\, kJ_0(kr)dk, \\ \sigma_{zz}(r,z) = \int_0^\infty \tau_{zz}(k,z)\, kJ_0(kr)dk, & \sigma_{rz}(r,z) = \int_0^\infty \tau_{rz}(k,z)\, kJ_1(kr)dk. \end{array} \tag{25}$$

These displacements and stresses satisfy the stress-strain relation and the wave equation in cylindrical coordinates with axial symmetry. These equations can be arranged to yield (Takeuchi and Saito, 1972):

$$\begin{aligned} \frac{\partial U_z}{\partial z} &= -\frac{c_{13}}{c_{33}}\left(\frac{\partial U_r}{\partial r} + \frac{U_r}{r}\right) + \frac{1}{c_{33}}\sigma_{zz}, \\ \frac{\partial U_r}{\partial z} &= -\frac{\partial U_z}{\partial r} + \frac{1}{c_{44}}\sigma_{rz}, \\ \frac{\partial \sigma_{zz}}{\partial z} &= -\rho\omega^2 U_z\left(\frac{\partial \sigma_{rz}}{\partial r} + \frac{\sigma_{rz}}{r}\right), \\ \frac{\partial \sigma_{rz}}{\partial z} &= \left(-c_{11} + \frac{c_{13}^2}{c_{33}}\right)\frac{\partial}{\partial r}\left(\frac{\partial U_r}{\partial r} + \frac{U_r}{r}\right) - \frac{c_{13}}{c_{33}}\frac{\partial \sigma_{zz}}{\partial r} - \rho\omega^2 U_r, \end{aligned} \tag{26}$$

which reduce to equations for the unknown integrands in Equation (25). Written in a matrix form, they are

$$\frac{\partial}{\partial z}\begin{bmatrix} u_r \\ u_z \\ \tau_{zz} \\ \tau_{rz} \end{bmatrix} = \begin{bmatrix} 0 & k & 0 & \frac{1}{c_{44}} \\ -k\frac{c_{13}}{c_{33}} & 0 & \frac{1}{c_{33}} & 0 \\ 0 & -\rho\omega^2 & 0 & -k \\ k^2\left(c_{11} - \frac{c_{13}^2}{c_{33}}\right) - \rho\omega^2 & 0 & k\frac{c_{13}}{c_{33}} & 0 \end{bmatrix}\begin{bmatrix} u_r \\ u_z \\ \tau_{zz} \\ \tau_{rz} \end{bmatrix}. \tag{27}$$

The solution of this differential equation is

$$(u_r, u_z, \tau_{zz}, \tau_{rz})^T = D_4 e^{\Lambda_4(z-z')} D_4^{-1}(u_r^0, u_z^0, \tau_{zz}^0, \tau_{rz}^0)^T, \tag{28}$$

where Λ_4 and D_4 are the eigenvalue and the eigenvector matrices of the coefficient matrix in Equation (27). The four eigenvalues are

$$\nu_{1,2} = i\nu_{a,b}, \quad \nu_{3,4} = -i\nu_{a,b}. \tag{29}$$

The corresponding eigenvector (column vector) matrix and its inverse are

$$D_4 = \begin{bmatrix} 1 & 1 & 1 & 1 \\ -x_2^a & -x_2^b & x_2^a & x_2^b \\ x_3^a & x_3^b & x_3^a & x_3^b \\ -x_4^a & -x_4^b & x_4^a & x_4^b \end{bmatrix}, \quad D_4^{-1} = \begin{bmatrix} px_3^b & qx_4^b & -p & -qx_2^b \\ -px_3^a & -qx_4^a & p & qx_2^a \\ px_3^b & -qx_4^b & -p & qx_2^b \\ -px_3^a & qx_4^a & p & -qx_2^a \end{bmatrix}. \tag{30}$$

where,

$$x_2^{a,b} = \frac{-ik\nu_{a,b}(c_{13}+c_{44})}{\rho\omega^2 - k^2c_{44} - c_{33}\nu_{a,b}^2}, \quad x_3^{a,b} = kc_{13} + ic_{33}\nu_{a,b}x_2^{a,b},$$

$$x_4^{a,b} = c_{44}(i\nu_{a,b} - kx_2^{a,b}), \quad p = \frac{0.5}{x_3^b - x_3^a}, \quad q = \frac{0.5}{x_4^a x_2^b - x_4^b x_2^a}.$$

If the positive z-axis is chosen to point downward, the first two columns of D_4 and the first two rows of D_4^{-1} correspond to the up-going P and S waves. The others are for the down-going waves.

The stress-displacement vector, $(u_r, u_z, \tau_{zz}, \tau_{rz})^T$, represents the z-dependent part of displacements and stresses at level z due to up and down-going $P-SV$ waves. If the amplitudes of these waves are represented by wave vector $\mathbf{v}_4$, with $\mathbf{v}_4 = (P_u, SV_u, P_d, SV_d)^T$, the stress-displacement vector can be written as

$$(u_r, u_z, \tau_{zz}, \tau_{rz})^T = D_4(z)\mathbf{v}_4(z). \tag{31}$$

That is, the contribution of each wave to the displacements and stresses is allocated according to the eigenvector or the direction of propagation of each wave. The relation between wave vectors on both sides of an interface separating two different TI media follows from the boundary conditions of two media in welded contact: the continuity of the stress-displacement vector $(u_r, u_z, \tau_{zz}, \tau_{rz})^T$. Thus, we have

$$\mathbf{v}_4(z_i^+) = D_4^{-1}(z_i^+)D_4(z_i^-)\mathbf{v}_4(z_i^-), \tag{32}$$

where, z_i^+ denotes the side above the interface and z_i^- below the interface.

Reflection and Transmission Coefficients

The relations in Equation (32) can be used to obtain the reflection and transmission coefficients of down-going and up-going waves at an interface (e.g., Mandal, 1991). If these reflection and transmission coefficients are denoted by 2×2 matrices R_d, T_d, R_u and T_u, we have

$$\begin{bmatrix} P_u^+ \\ SV_u^+ \\ P_d^+ \\ SV_d^+ \end{bmatrix} = \begin{bmatrix} R_d & T_u \\ \mathbf{1} & \mathbf{0} \end{bmatrix} \begin{bmatrix} P_d^+ \\ SV_d^+ \\ P_u^- \\ SV_u^- \end{bmatrix}, \quad \begin{bmatrix} P_u^- \\ SV_u^- \\ P_d^- \\ SV_d^- \end{bmatrix} = \begin{bmatrix} \mathbf{0} & \mathbf{1} \\ T_d & R_u \end{bmatrix} \begin{bmatrix} P_d^+ \\ SV_d^+ \\ P_u^- \\ SV_u^- \end{bmatrix}. \tag{33}$$

In the above, the 2×2 zero and identity matrices are represented by $\mathbf{0}$ and $\mathbf{1}$. Substituting Equation (33) into Equation (32) and defining W (4×4) as the resultant matrix of $D_4^{-1}(z_i^+)D_4(z_i^-)$, we then have

$$\begin{bmatrix} R_d & T_u \\ T_d & R_u \end{bmatrix} = \begin{bmatrix} W_{12}W_{22}^{-1} & W_{11} - W_{12}W_{22}^{-1}W_{21} \\ W_{22}^{-1} & -W_{22}^{-1}W_{21} \end{bmatrix}. \tag{34}$$

The 2×2 submatrices of the 4×4 matrix W are represented by W_{11}, W_{12}, W_{21} and W_{22}. Equation (34) applies only to a single interface separating two half spaces. These are the simple reflection or transmission coefficients. To calculate the generalized reflection and transmission coefficient for a stack of layers, the reflectivity method (Kennet, 1983; Müller, 1985) can be followed.

Initial Wave Amplitudes for the Reflectivity Method

As indicated by Equation (31), the wave amplitudes can be obtained by applying the inverse eigenvector operator to the stress-displacement vector of the direct waves, which are given by Equations (12) through (19). This yields the following simple expressions for the up- and down-going direct P and SV wave amplitudes for the vertical and radial ring forces.

$$\begin{bmatrix} P_u \\ SV_u \\ P_d \\ SV_d \end{bmatrix}_v = D_4^{-1} \begin{bmatrix} u_r \\ u_z \\ \tau_{zz} \\ \tau_{rz} \end{bmatrix}_v = \begin{bmatrix} -pe^{-i\nu_a(z-z')} \\ pe^{-i\nu_b(z-z')} \\ pe^{i\nu_a(z-z')} \\ -pe^{i\nu_b(z-z')} \end{bmatrix} r_0 J_0(kr_0), \tag{35}$$

$$\begin{bmatrix} P_u \\ SV_u \\ P_d \\ SV_d \end{bmatrix}_r = D_4^{-1} \begin{bmatrix} u_r \\ u_z \\ \tau_{zz} \\ \tau_{rz} \end{bmatrix}_r = \begin{bmatrix} -qx_2^b e^{-i\nu_a(z-z')} \\ qx_2^a e^{-i\nu_b(z-z')} \\ -qx_2^b e^{i\nu_a(z-z')} \\ qx_2^a e^{i\nu_b(z-z')} \end{bmatrix} r_0 J_1(kr_0). \tag{36}$$

In the BEM implementation, Equations (35) and (36) need to be integrated over the source position z' for the wall elements. The results of these integrations are the input to the reflectivity program.

INCORPORATION OF FLUID, CASING, AND CEMENT

When casing and cement are installed in a borehole, the original fluid column changes to a cylindrically layered isotropic medium. Similarly to the case of a plane layered medium, wave propagation in the cylindrically layered medium can be studied by rewriting the wave equation into an ordinary differential equation for the displacement-stress vector. Nevertheless, it is more expedient to work with potentials because of the isotropic nature of each layer. Furthermore, for the plane layered medium displacements are expressed as horizontal wave number integrals so as to satisfy the phase-matching condition at the interfaces. For the cylindrically layered medium, the phase-matching condition is satisfied by expressing the potentials as integrals over the vertical wave number. Let A_s, B_s, A_o, and B_o represent the amplitudes of the incoming (standing) and outgoing P and S wave potentials in any solid layer, C_s and C_o be the corresponding potential amplitudes for the P wave in any fluid layer, then the potentials assume the following form

$$\begin{aligned} \phi &= \tfrac{1}{2\pi} \textstyle\int_{-\infty}^{\infty} [A_s I_0(\xi_a r) + A_o K_0(\xi_a r)] e^{ik_z(z-z')} dk_z, \\ \psi &= \tfrac{1}{2\pi} \textstyle\int_{-\infty}^{\infty} [B_s I_1(\xi_b r) + B_o K_1(\xi_b r)] e^{ik_z(z-z')} dk_z, \\ \phi_f &= \tfrac{1}{2\pi} \textstyle\int_{-\infty}^{\infty} [C_s I_0(\xi_f r) + C_o K_0(\xi_f r)] e^{ik_z(z-z')} dk_z. \end{aligned} \tag{37}$$

where,

$$\xi_a = i\sqrt{k_a^2 - k_z^2}, \quad \xi_b = i\sqrt{k_b^2 - k_z^2}, \quad \xi_f = i\sqrt{k_f^2 - k_z^2},$$

and k_a, k_b, and k_f are the total P and S wavenumbers in the solid and P wavenumber in the fluid. Using the following relationship between displacements and potentials,

$$u_r = \frac{\partial \phi}{\partial r} - \frac{\partial \psi}{\partial z}, \quad u_z = \frac{\partial \phi}{\partial z} + \frac{\partial (r\psi)}{r \partial r}, \tag{38}$$

the displacements-stress vectors in the solid and fluid are

$$(u_r, u_z, \tau_{rr}, \tau_{rz})^T = S(r)\mathbf{v}_4, \quad (u_r, u_z, \tau_{rr}, \tau_{rz})^T = F(r)\mathbf{v}_2, \tag{39}$$

where, $\mathbf{v}_4 = (A_s, B_s, A_o, B_o)^T$ and $\mathbf{v}_2 = (C_s, C_o)^T$ are the amplitude vectors. From matrices S and F, the reflection and transmission coefficients of P and S waves at the solid-solid and solid-fluid interfaces can be readily obtained. The procedure for the solid-solid contact is the same as in the previous section. The solid-fluid contact case is illustrated in the following.

Reflection and Transmission Coefficients

For an interface at $r = r_0$ between a fluid column ($r < r_0$) and an elastic formation ($r > r_0$), the following equations hold

$$\begin{bmatrix} A_s \\ B_s \\ A_o \\ B_o \end{bmatrix} = \begin{bmatrix} 1 & 0 & 0 \\ 0 & 1 & 0 \\ R^i_{pp} & R^i_{sp} & T^o_{pp} \\ R^i_{ps} & R^i_{ss} & T^o_{ps} \end{bmatrix} \begin{bmatrix} A_s \\ B_s \\ C_o \end{bmatrix}, \quad \begin{bmatrix} C_s \\ C_o \end{bmatrix} = \begin{bmatrix} T^i_{pp} & T^i_{sp} & R^o_{pp} \\ 0 & 0 & 1 \end{bmatrix} \begin{bmatrix} A_s \\ B_s \\ C_o \end{bmatrix}. \tag{40}$$

The above equations simply state that the outgoing P and S waves in the formation result from the reflection of incoming P and S waves in the formation, plus the transmission of an outgoing P wave in the fluid. An incoming P wave in the fluid is the consequence of an outgoing P wave reflection and an incoming P and S wave transmission. Substituting Equation (40) into Equation (39) and applying the three boundary conditions, we obtain

$$\begin{bmatrix} S_{11} & S_{12} & S_{13} & S_{14} \\ S_{31} & S_{32} & S_{33} & S_{34} \\ S_{41} & S_{42} & S_{43} & S_{44} \end{bmatrix} \begin{bmatrix} 1 & 0 & 0 \\ 0 & 1 & 0 \\ R^i_{pp} & R^i_{sp} & T^o_{pp} \\ R^i_{ps} & R^i_{ss} & T^o_{ps} \end{bmatrix} = \begin{bmatrix} F_{11} & F_{12} \\ F_{31} & F_{32} \\ F_{41} & F_{42} \end{bmatrix} \begin{bmatrix} T^i_{pp} & T^i_{sp} & R^o_{pp} \\ 0 & 0 & 1 \end{bmatrix}. \tag{41}$$

The nine unknown coefficients can be obtained from the nine equations implied by Equation (41). These coefficients can in turn be used in the reflectivity method for cylindrical layered media.

If $r > r_0$ is the fluid region and $r < r_0$ the solid region, the resulting equation for the coefficients differs from Equation (41) only in the column position of the S and F matrices, the individual coefficients can be readily obtained by corresponding element substitution.

Initial Potential of Element Sources

Upon expressing the scalar Green's functions of Equation (4) in terms of modified Bessel functions, and then comparing the resultant displacement for vertical and radial ring sources with Equation (38), the initial potentials can be obtained. For a vertical ring

force, the radial displacement is

$$U_r = \frac{\partial}{\partial r}\left(2ir_0\int_{-\infty}^{\infty} k_z[K_0(\xi_b r_0)I_0(\xi_b r) - K_0(\xi_a r_0)I_0(\xi_a r)]e^{ik_z(z-z')}dk_z\right). \quad (42)$$

A comparison of this result with Equation (38) yields immediately the P and SV wave potentials due to a vertical ring force. They are

$$\begin{aligned}\phi_v^c &= \tfrac{-ir_0}{2\pi\rho\omega^2}\textstyle\int_{-\infty}^{\infty} k_z K_0(\xi_a r_0)I_0(\xi_a r)e^{ik_z(z-z')}dk_z,\\ \psi_v^c &= \tfrac{-r_0}{2\pi\rho\omega^2}\textstyle\int_{-\infty}^{\infty} \xi_b K_0(\xi_b r_0)I_1(\xi_b r)e^{ik_z(z-z')}dk_z.\end{aligned} \quad (43)$$

For a radial ring force, the vertical displacement is

$$\begin{aligned}U_z &= \frac{\partial}{\partial z}\left(\frac{-r_0}{2\pi\rho\omega^2}\int_{-\infty}^{\infty}\xi_a K_1(\xi_a r_0)I_0(\xi_a r)e^{ik_z(z-z')}dk_z\right)\\ &\quad +\frac{1}{r}\frac{\partial}{\partial r}\left(\frac{ir_0}{2\pi\rho\omega^2}\int_{-\infty}^{\infty}k_z K_1(\xi_b r_0)I_0(\xi_b r)e^{ik_z(z-z')}dk_z\right).\end{aligned} \quad (44)$$

Thus, a comparison with Equation (38) gives the P and SV wave potentials produced by a radial ring source

$$\begin{aligned}\phi_r^c &= \tfrac{-r_0}{2\pi\rho\omega^2}\textstyle\int_{-\infty}^{\infty}\xi_a K_1(\xi_a r_0)I_0(\xi_a r)e^{ik_z(z-z')}dk_z,\\ \psi_r^c &= \tfrac{ir_0}{2\pi\rho\omega^2}\textstyle\int_{-\infty}^{\infty}k_z K_1(\xi_b r_0)I_1(\xi_b r)e^{ik_z(z-z')}dk_z.\end{aligned} \quad (45)$$

These expressions provide the incident potential amplitude at the outer cylindrical interface. The products (matrix multiplication) of these incident potentials with the reflection and transmission coefficient matrices yield the reflected potentials in the solid layer and transmitted potentials in the fluid. The total potentials then yield the total displacements and stresses used for matching boundary conditions and for program output.

THE INITIAL DATA AT THE ELEMENTS

To solve the system of equations in Equation (6) for the fictitious sources on each element, the initial displacements and stresses directly due to the physical source are required. They appear on the right hand side of the system of equations. These data depend on the type of sources used and whether or not the borehole is cased. We consider three conventional sources here: the explosive volume source, the axial source, and the radial source. In practice, they correspond to an air gun or dynamite, wall-clamped vibrators, and a bender source or cavity resonator, respectively.

Sources in an Open Borehole

For sources in an open borehole, empty or fluid-filled, either the physical source or its direct wavefield is in contact with the formation. With the axial and radial sources, the vibrating forces are applied directly at the boundary of interest. Thus, the initial data

for these two sources are just the driving forces applied to the elements. The initial data for the displacements are set to zero. For an explosive source at the center of a fluid-filled borehole, the initial data at the boundary are

$$\begin{aligned} U_r &= \frac{V_s}{4\pi} i \int_0^\infty \frac{k^2}{\nu_f} J_1(kr_0) e^{i\nu_f|z-z_s|} dk, \\ \sigma_{rr} &= \frac{V_s}{4\pi\rho_f\omega^2} i \int_0^\infty \frac{k}{\nu_f} J_0(kr_0) e^{i\nu_f|z-z_s|} dk, \\ \sigma_{rz} &= 0. \end{aligned} \tag{46}$$

The vertical position of the source and the element is z_s and z respectively. The strength of the volume source is denoted by V_s. The value of V_s for commonly used explosion sources is about 1600 cm^3.

Sources in a Cased Borehole

In a cased borehole, the sources and their direct fields are not in direct contact with the boundary elements. The initial data is influenced by the casing and the cement. Since the cement and formation are in welded contact, four boundary conditions have to be satisfied. Consequently, four pieces of data are needed on each element. In what follows, we present the P and S potentials that can be used to derive the displacements and stresses by applying matrix $S(r_0)$ to their amplitudes, as indicated by Equation (39).

The two potentials due to a volume source of strength V_s are

$$\begin{aligned} \phi &= \frac{V_s}{4\pi^2} \int_{-\infty}^{\infty} \overline{T}^o_{pp} \, K_0(\xi_a r_0) e^{ik_z(z-z')} dk_z, \\ \psi &= \frac{V_s}{4\pi^2} \int_{-\infty}^{\infty} \overline{T}^o_{ps} \, K_1(\xi_b r_0) e^{ik_z(z-z')} dk_z, \end{aligned} \tag{47}$$

where, $\overline{T}^o_{pp}$ and $\overline{T}^o_{ps}$ are the *overall* $P-P$ and $P-S$ transmission coefficients from the fluid to the elements.

To obtain data for the other two sources, let us first define a 4×4 matrix, E,

$$E = S(r_1) S^{-1}(r_2^-) S(r_2^+), \tag{48}$$

where, S is the matrix defined in Equation (39), and r_1 and r_2 are the inner and outer radii of the casing. Then, the potentials at the boundary element and in the fluid, due to an axial force applied on the casing over a depth range of $2l$ and centered at z_s, are

$$\begin{aligned} \phi &= \frac{1}{2\pi} \int_{-\infty}^{\infty} \frac{F_{11}E_{34} - F_{31}E_{14}}{DET} F(k_z) K_0(\xi_a r_0) e^{ik_z(z-z_s)} dk_z, \\ \psi &= \frac{1}{2\pi} \int_{-\infty}^{\infty} \frac{F_{11}E_{33} - F_{31}E_{13}}{DET} F(k_z) K_1(\xi_b r_0) e^{ik_z(z-z_s)} dk_z, \\ \phi_f &= \frac{1}{2\pi} \int_{-\infty}^{\infty} \frac{E_{13}E_{34} - E_{14}E_{33}}{DET} F(k_z) I_0(\xi_f r) e^{ik_z(z-z_s)} dk_z. \end{aligned} \tag{49}$$

E_{ij} in the above is the corresponding (i,j) element of the E matrix, and $DET = F_{11}(E_{43}E_{34} - E_{33}E_{44}) + F_{31}(E_{13}E_{44} - E_{14}E_{43})$. Function $F(k_z) = 2l\mathrm{sinc}(k_z l)$ represents the source spectrum. Similarly, the potentials for the radial source are

$$\begin{aligned} \phi &= \frac{1}{2\pi} \int_{-\infty}^{\infty} \frac{-F_{11}E_{44}}{DET} F(k_z) K_0(\xi_a r_0) e^{ik_z(z-z_s)} dk_z, \\ \psi &= \frac{1}{2\pi} \int_{-\infty}^{\infty} \frac{F_{11}E_{31}}{DET} F(k_z) K_1(\xi_b r_0) e^{ik_z(z-z_s)} dk_z, \\ \phi_f &= \frac{1}{2\pi} \int_{-\infty}^{\infty} \frac{E_{14}E_{43} - E_{13}E_{44}}{DET} F(k_z) I_0(\xi_f r) e^{ik_z(z-z_s)} dk_z. \end{aligned} \tag{50}$$

It should be pointed out that when pressure in the fluid is calculated from the fictitious sources on the boundary, the resulting pressure is only part of the solution. The total pressure in the fluid should include the casing reflection from the direct wavefield in the case of the volume source. In the case of the axial and the radial sources, direct contributions from the source to the pressure field should be added, because this part of the wavefield did not contribute to the BEM fictitious source solution on the boundary.

MORE ON BEM IMPLEMENTATION

Once the circular source results are incorporated into the reflectivity scheme, the end products are two wavenumber integrals, a horizontal wavenumber integral for the plane layered isotropic or anisotropic formation, and a vertical wavenumber integral for the cylindrically layered isotropic medium. Since integral over element height depends on wavenumbers, its evaluation must precede the wavenumber integration. The integration over the source element coordinate, z', for plane layers is of two types: integral of a complex exponential, and integral of a sign function multiplied by the exponential function. Both can be integrated analytically.

An exact analytical evaluation of the wavenumber integrals (both k and k_z) is impossible, and a numerical method is necessary. Bessel functions J_0 and J_1 in the k integrals suggest the use of fast Hankel transform algorithms. Unfortunately, one cannot employ these fast algorithms because the upper bound of the wavenumber is not known for a certain accuracy specification. That is, given an accuracy requirement for the integrated results, one cannot predict up to which wavenumber the inputs to these algorithms should be prepared. Thus, the only alternative is to evaluate these integrals by discrete summation for many wavenumbers. This is the so-called *Discrete Wavenumber Method* (Bouchon and Aki, 1977).

In wavenumber summation, the convergence of the partial sums are tested using asymptotic approximations. This is because the integrands are oscillatory functions of the wavenumber. Instead of the actual N-th term, the modulus of its asymptotic expression is used to compare with the partial sum. If the ratio of the N-th term to the partial sum is smaller than the specified accuracy, summation is stopped.

EXAMPLES

BEM results for a borehole in a homogeneous TI medium are first checked against those from a discrete wavenumber (DWN) calculation. Then, the technique is used to illustrate the effect of a borehole, either open or cased, in a three-layer medium.

BEM vs. DWN: Waveform Comparison

Figure 4 shows the radial (U_R) and tangential (U_0) displacements in a TI formation computed by the BEM and DWN methods. The waveforms calculated by two totally

different numerical methods agree with each other very well. The elastic parameters of the formation are: $c_{11} = 50.78$, $c_{33} = 36.85$, $c_{13} = 21.49$, $c_{44} = 11.01$, $c_{66} = 14.87$, $\rho = 2.56$. The wavefield is recorded by a circular receiver array which is 40 m from the explosion source placed in a water-filled open borehole of radius $r_0 = 0.1$ m. The strong P-wave anisotropy is clearly shown in Figure 4 by the different arrival time for P waves traveling in different directions. The large contribution of a *quasi-SV* wave on the U_R section, and the negligible *quasi-P* energy on the U_θ section, agree with what has been discussed in Dong and Toksöz (1993). That is, the dilatational component of the *quasi-SV* wave is on the same order as that of the *quasi-P* wave. The rotational component of the *quasi-P* wave is two orders of magnitude smaller than that of the *quasi-SV* wave.

Borehole in Three-Layer Media

When a fluid-filled borehole is inside a layered isotropic or anisotropic medium, the tube waves, excited by the source and propagating along the borehole, will interact with the vertical inhomogeneities. This interaction results in wave scattering and conversion along the path of the tube wave. The phenomenon is illustrated here through a few examples.

Figure 5 shows the solid displacements for volume, radial, and vertical sources in a water-filled borehole embedded in a three-layer isotropic medium. The medium parameters of this example are taken from Bouchon (1993) and listed in Table 1. The sources are located 2 m above the low velocity layer. And the vertical geophone array (1 m vertical offset from the source) is 4 m away from the borehole axis. Center frequency of the Ricker wavelet is 2.5 kHz. In addition to the primary P and S waves in the displacement seismograms, which are normally observable if the borehole is absent, strong events appear at a later time and with energy concentrated in the second and third layer. Comparing to volume and radial sources which are efficient tube wave generators, the vertical source induces a much lower amount of tube wave energy. The fact that these late arrivals are much weaker for vertical source illustrate that they are of tube wave origin and trapped in the second layer as guided modes.

Figure 6 displays the time response of the diffracting sources on the borehole boundary for the three physical borehole sources in the three-layer medium. The diagrams represent the source borehole radiation into the formation and specify uniquely how a borehole source could be equivalently approximated. The reflection of a tube wave at the upper and lower interfaces of the low velocity zone is clearly indicated in these figures. Because of these reverbrations, the part of the borehole embedded in the low velocity layer radiates energy into the formation for a long time. In agreement with the observation from Figure 6, the equivalent sources within the low velocity layer are relatively weaker for the vertical source than for the other two sources. The reflections from the top and bottom of each figure result from the finite borehole length used in the calculation.

In the next three cases (see Table 1 for parameters), the parameters of the first and third layers remain unchanged, while the parameters of the second layer vary.

Figure 7 shows the displacements due to volume source when the second layer is a soft TI formation, a harder isotropic formation, and a hard isotropic formation. When the velocities of the second layer are increased, the trapped energy decreases, and it disappears when the velocities are very high. This illustrates that tube wave conversion is mainly associated with low velocity channels. In the case of a TI second layer (Test #1), the overall appearance of the displacement sections is similar to that of Figure 5. On the other hand, differences do exist due to anisotropy. For instance, in the isotropic case, particle motion of shear wave is perpendicular to the direction of its propagation (almost vertical due to large shear wave velocity contrast), resulting in large U_r and small U_z. In the anisotropic case, however, directions of particle motion and propagation are no longer perpendicular. In our case, the particle motion tends to align toward vertical, leading to larger U_z. Another difference is that the trapped modes in the TI case tend to spread out and have recognizable separation in time.

The displacements for a volume source in a cased borehole are shown in Figure 8. The medium parameters of the TI case in Figure 7 are used. Comparison with Figure 7 shows that the amplitude of the trapped energy is relatively larger in Figure 8. This illustrates the fact that casing and cement reduce the amplitude of primary body waves, while they only slightly affect the tube wave and its conversions.

CONCLUSIONS

The BEM-discrete wavenumber modeling method is extended to include transverse isotropy and cased boreholes. The method overcomes the problem of scale associated with other numerical methods in the borehole environment. It is especially suitable for modeling wave radiation and propagation from or inside a fluid-filled borehole, open or cased. The method is semi-analytical in the sense that the only discretization occurs on the borehole wall, and wave propagation is realized through the analytical Green's function of the layered TI medium outside the borehole, and through the isotropic Green's function for cylindrical layers inside the borehole. Comparison of the BEM results with their discrete wavenumber counterparts validates the implementation. Tests on several three-layer media show the importance of low velocity layers in the tube wave interaction with the surrounding formation. The by-product of the method - fictitious boundary sources - can be used to study approximations for actual borehole sources.

ACKNOWLEDGEMENTS

This work was supported by U.S. Department of Energy grant #DE-FG02-89ER14084.

REFERENCES

Banerjee, P.K. and R. Butterfield, 1981, *Boundary Element Methods in Engineering Science*, McGraw-Hill Book Co. Ltd., London.

Bouchon, M., 1993, A numerical simulation of the acoustic and elastic wavefields radiated by a source in a fluid-filled borehole embedded in a layered medium, *Geophysics, 58*, 475–481.

Bouchon, M. and K. Aki, 1977, Discrete wave-number representation seismic-source wave fields, *Bull. Seis. Soc. Am., 67*, 259–277.

Bouchon, M. and D.P. Schmitt, 1989, Full-wave acoustic logging in an irregular borehole, *Geophysics, 54*, 758–765.

Brebbia, C.A. and J. Dominguez, 1989, *Boundary Elements: An Introductory Course*, McGraw-Hill Inc., New York.

Cheng, C.H. and M.N. Toksöz, 1981, Elastic wave propagation in a fluid-filled borehole and synthetic acoustic logs, *Geophysics*, **46**, 1042–1053.

Dong, W., 1993, Elastic wave radiation from borehole seismic sources in anisotropic media, Ph.D. thesis, MIT.

Dong, W. and D.P. Schmitt, 1993, Simplified dynamic and static Green's functions in transversely isotropic media, submitted to *Geophysical J. Intl.*.

Dong, W. and M.N. Toksöz, 1993, Borehole seismic source radiation patterns in transversely isotropic media: theoretical results, submitted to *Geophysics*.

Ellefsen, K.J., 1990, Elastic wave propagation along a borehole in an anisotropic medium, Sc.D. thesis, MIT.

Gibson, R.L., 1993, Radiation from seismic sources in cased and cemented boreholes, *Geophysics*, in press.

Kawase, H., 1988, Time domain response of a semicircular canyon for incident SV, P, and Rayleigh waves calculated by the discrete wavenumber boundary element method, *Bull. Seism. Soc. Am., 79*, 1361–1382.

Kennet, B.L.N., 1983, *Seismic Wave Propagation in Stratified Media*, Cambridge University Press, Cambridge.

Mandal, B., 1991, Reflection and transmission properties of elastic waves on a plane interface for general anisotropic media, *J. Acoust. Soc. Am., 90*, 1106–1118.

Meredith, J.A., 1990, Numerical and analytical modeling of downhole seismic sources: the near and far field, Ph.D. thesis, MIT.

Müller, G., 1985, The reflectivity method: A tutorial, *J. Geophys., 58*, 153–174.

Randall, C.J., D.J. Scheibner, and P.T. Wu, 1991, Multipole borehole acoustic waveforms: Synthetic logs with beds and borehole washouts, *Geophysics, 56*, 1757–1769.

Schmitt, D.P., 1989, Acoustic multipole logging in transversely isotropic poroelastic formations, *J. Acoust. Soc. Am., 86*, 2397–2421.

Schmitt, D.P. and M. Bouchon, 1985, Full-wave acoustic logging: Synthetic microseismograms and frequency-wavenumber analysis, *Geophysics, 50*, 1756–1778.

Schoenberg, M., T. Marzetta, J. Aron, and R. Porter, 1981, Space-time dependence of acoustic waves in a borehole, *J. Acoust. Soc. Am., 70*, 1496–1507.

Stephen, R.A., F. Pardo-Casas, and C.H. Cheng, 1985, Finite difference synthetic acoustic logs, *Geophysics, 50*, 1588–1609.

Takeuchi, H. and M. Saito, 1972, Seismic surface waves, in *Methods in Computational Physics*, Academic Press, New York, 11, 217–295.

Thomsen, L., Weak elastic anisotropy, *Geophysics, 51*, 1954–1966.

Tubman, K.M., C.H. Cheng, and M.N. Toksöz, 1984, Synthetic full-waveform acoustic logs in cased boreholes, *Geophysics, 49*, 1051–1059.

White, J.E. and C. Tongtaow, 1981, Cylindrical waves in transversely isotropic media, *J. Acous. Soc. Amer., 70*, 1147–1155.

Winbow, G.A., 1991, Seismic sources in open and cased boreholes, *Geophysics, 58*, 1001–1019.

tests	*borehole fluid*	*1st and 3rd layer*	*2nd layer*
Bouchon	$c_f = 1.5$, $\rho_f = 1$	$v_p = 3$, $v_s = 1.7$, $\rho = 2.7$	$v_p = 2$, $v_s = .85$, $\rho = 2.4$
Test #1	same	same	$c_{11} = 11.6$, $c_{33} = 9.6$ $c_{13} = 5.6$, $c_{44} = 1.5$ $c_{66} = 1.7$, $\rho = 2.4$
Test #2	same	same	$v_p = 3$, $v_s = 1.5$, $\rho = 2.0$
Test #3	same	same	$v_p = 5$, $v_s = 3.0$, $\rho = 2.3$
Cased	steel & cement	same	same as Test #1

Table 1: Parameters used for the three-layer model simulations. Units of velocity and density are km/s and g/cm^3. Elastic constants are in GPa. Borehole radius is 12 cm. For cased borehole, casing and cement are each 2 cm thick.

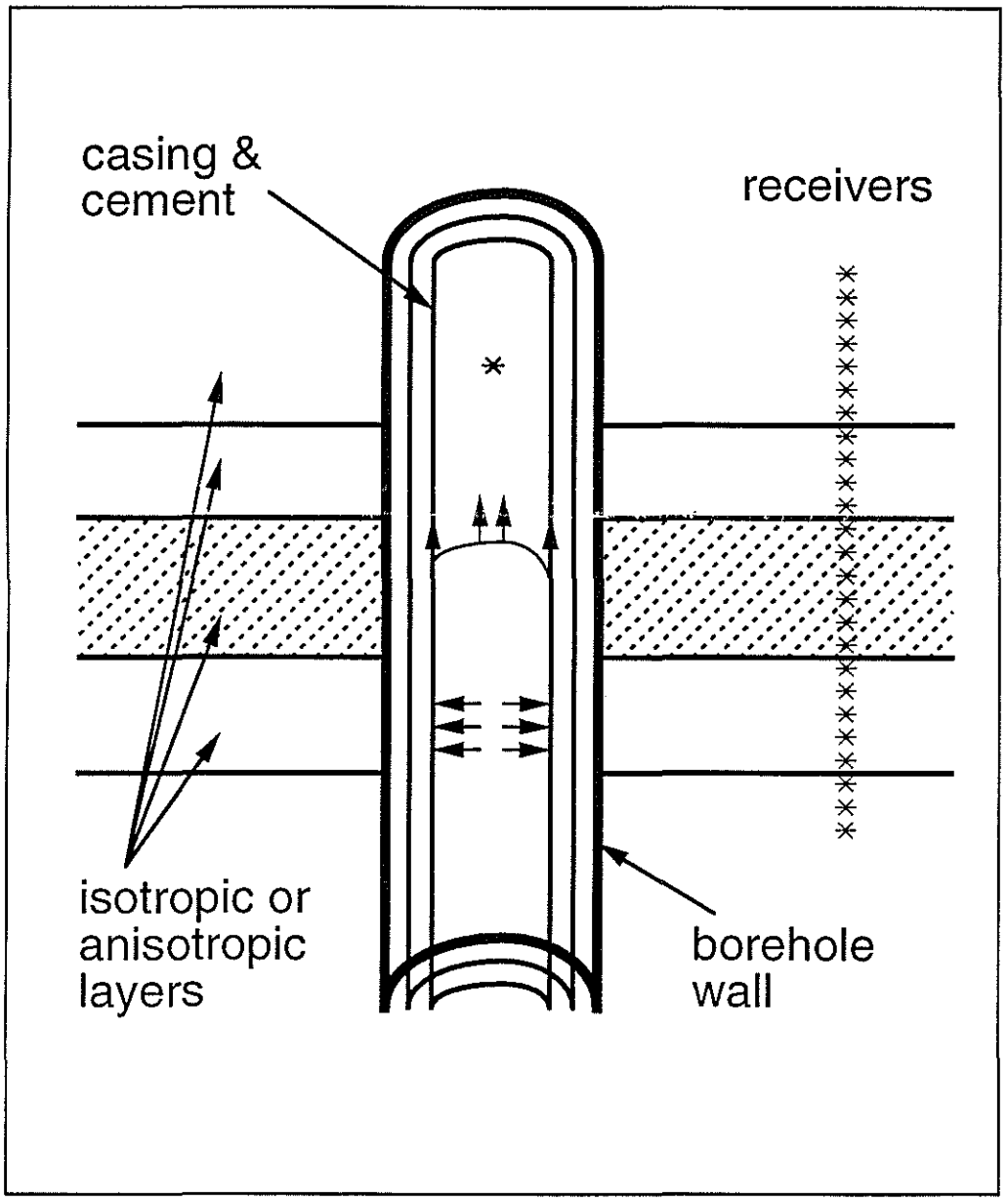

Figure 1: Problem configuration for a cased borehole in a layered transversely isotropic medium. Given a downhole source (explosion; vibrator; bender), the problem is to determine the fluid pressure inside the borehole and the displacements in the solid formation.

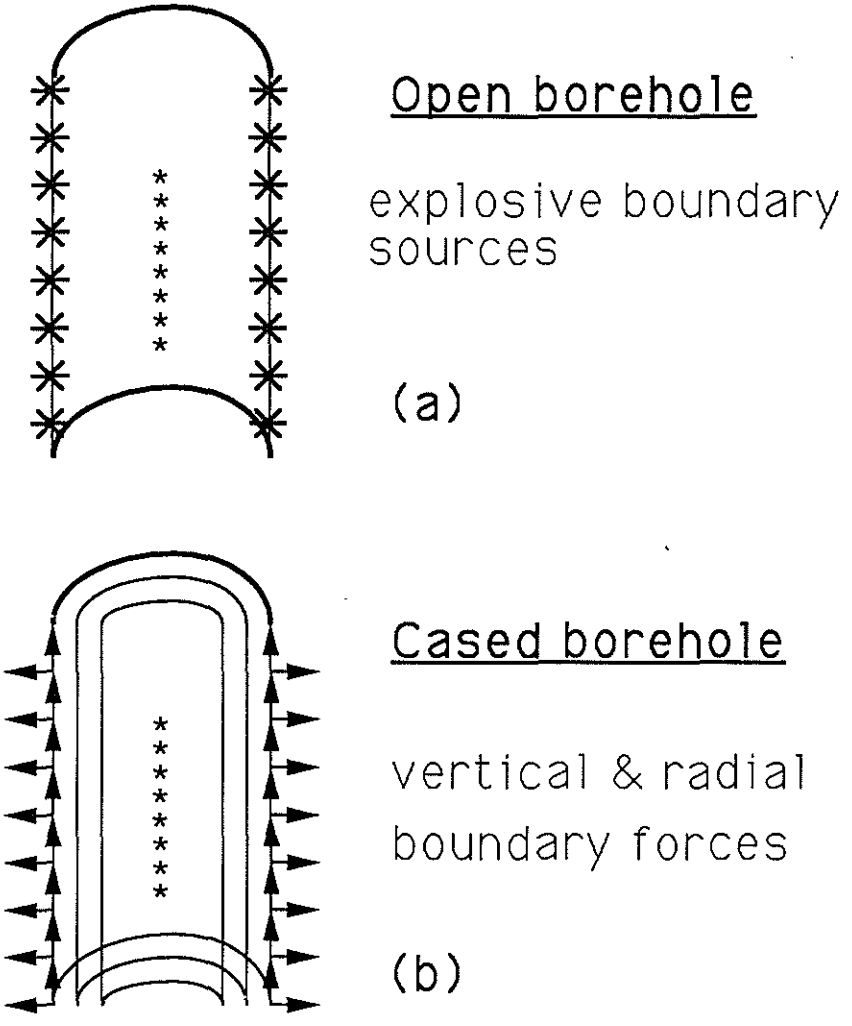

Figure 2: Equivalent problem for borehole fluid in an open borehole (a), and in a cased borehole (b). The effect of a solid formation on the wavefield is equivalent to a sheet of explosion sources at the borehole wall for case (a), and a sheet of vertical and radial forces at the wall for case (b). Once these assumed source sheets are known, pressure in the borehole fluid is readily computed.

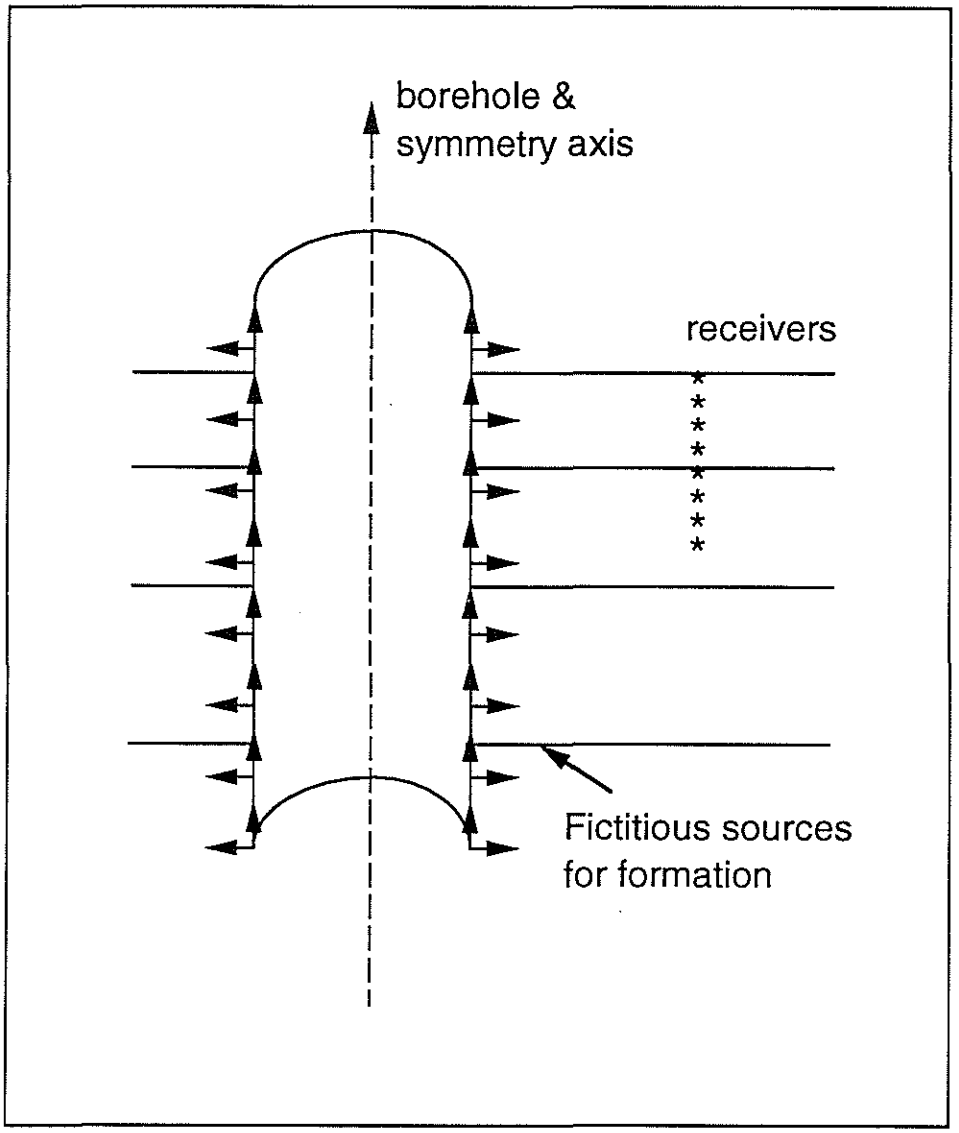

Figure 3: Equivalent problem for the layered formation in the cases of open and cased boreholes. The effect of the borehole fluid, casing, and cement on the out-going wavefield is equivalent to a sheet of vertical and radial forces at the wall. Once these assumed source sheets are known, displacements in the surrounding formation are readily obtained.

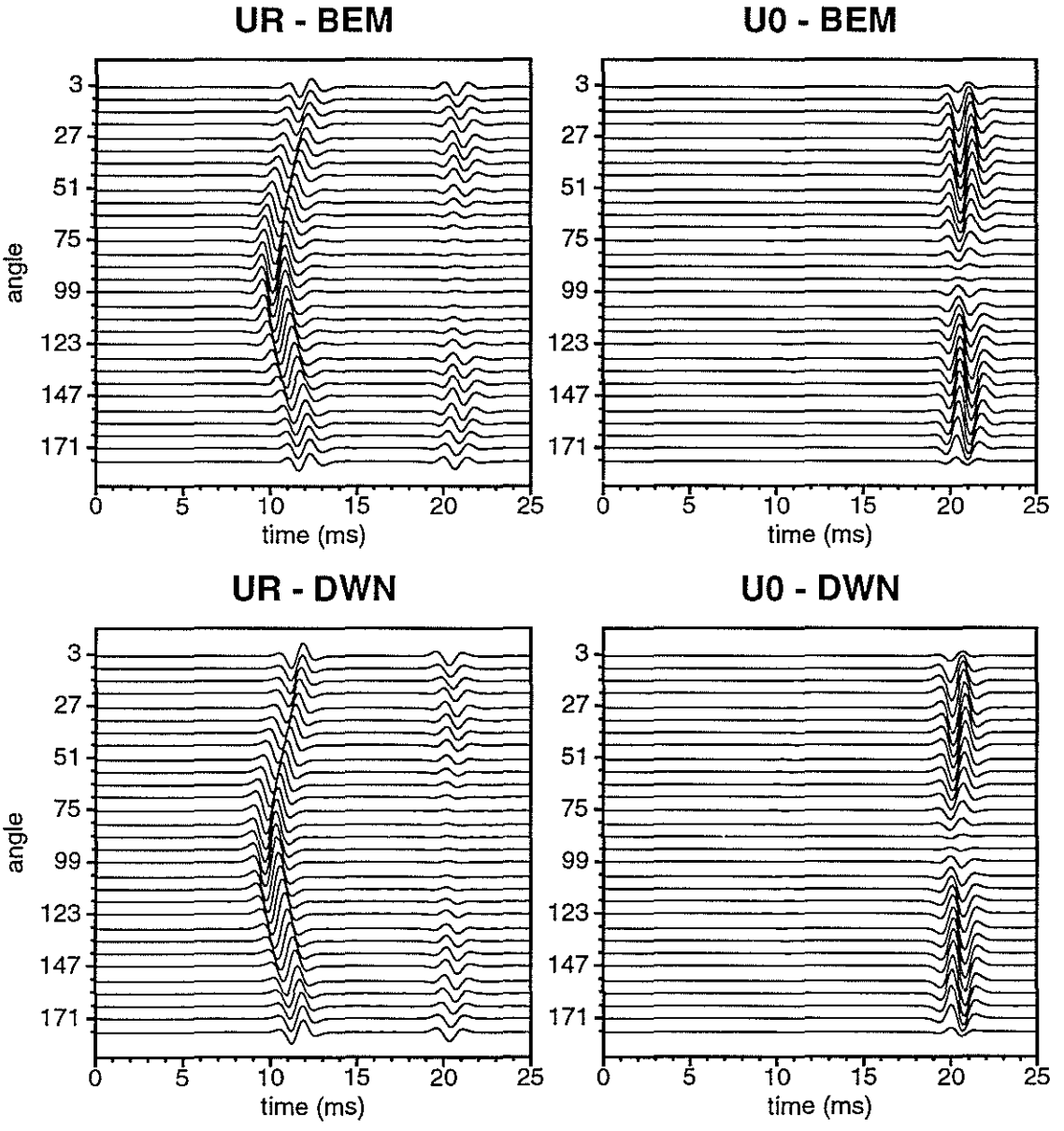

Figure 4: Comparison of BEM and DWN results for a volume source in a fluid-filled borehole embedded in a homogeneous TI medium. Parameters: $r_0 = 0.1$, $f_0 = 500\ Hz$, $R = 40\ m$, $c_{11} = 50.78$, $c_{33} = 36.85$, $c_{13} = 21.49$, $c_{44} = 11.01$, $c_{66} = 14.87$, $\rho = 2.56$, receiver array radius $R = 30\ m$.

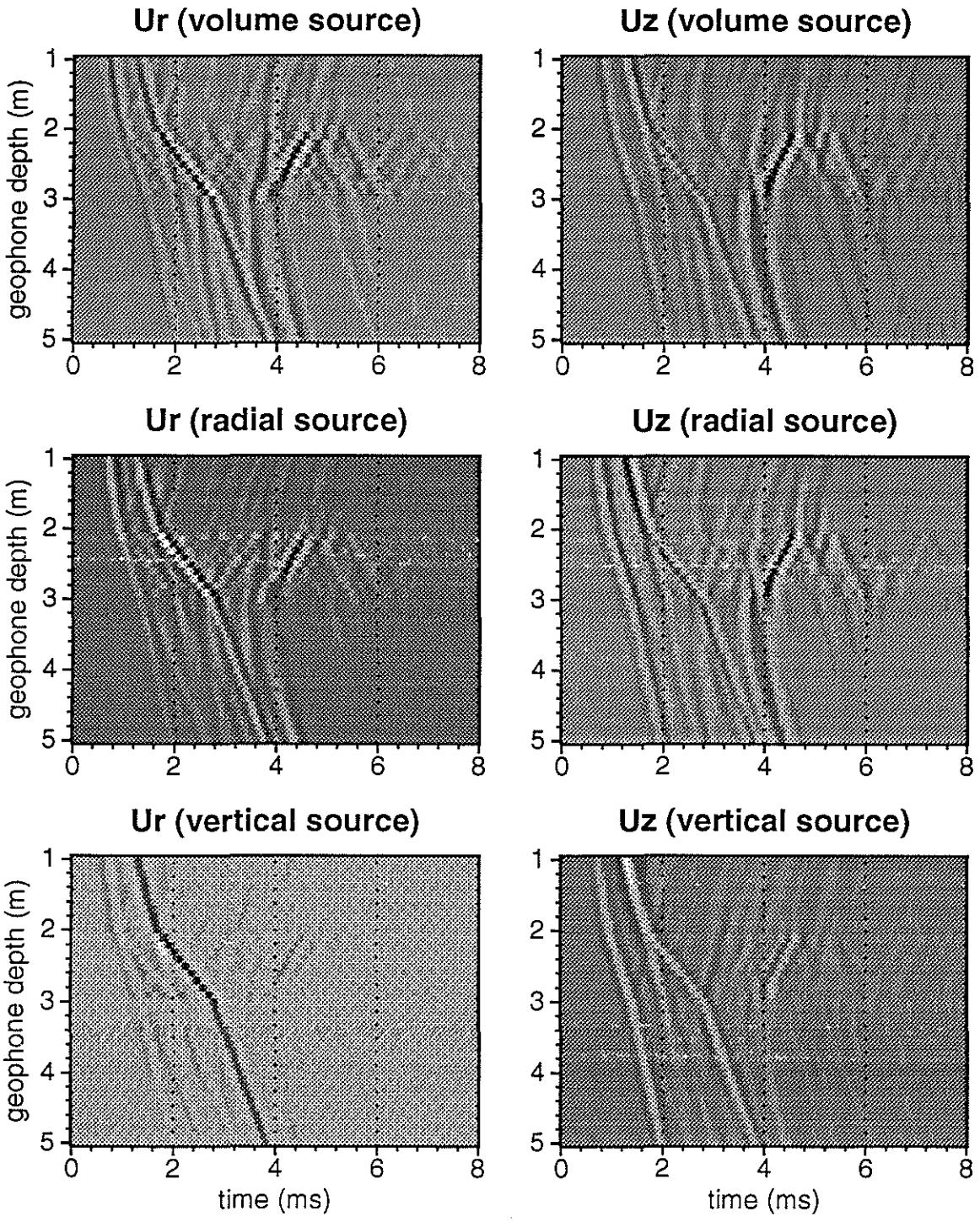

Figure 5: Horizontal and vertical displacements in the formation for volume, radial, and vertical sources in a fluid-filled borehole penetrating a three-layer isotropic medium.

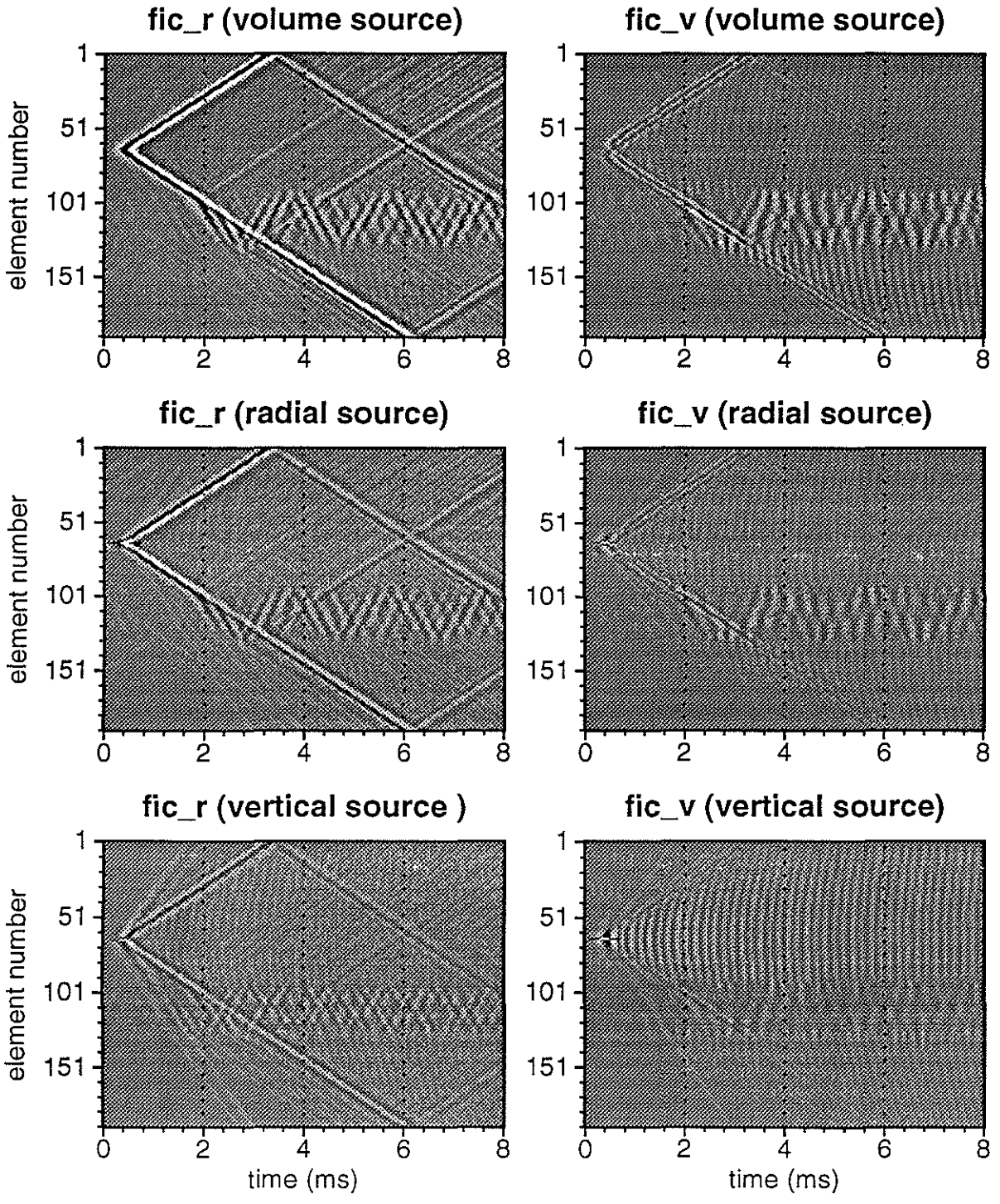

Figure 6: Equivalent time domain boundary sources (fic_r and fic_v for horizontal and vertical forces, respectively) for the physical sources in Figure 5. In studying these figures, one needs to be aware that the vertical coordinates are numbers of elements. Since the element height in the different layers is different, one cannot simply measure the velocity from these figures.

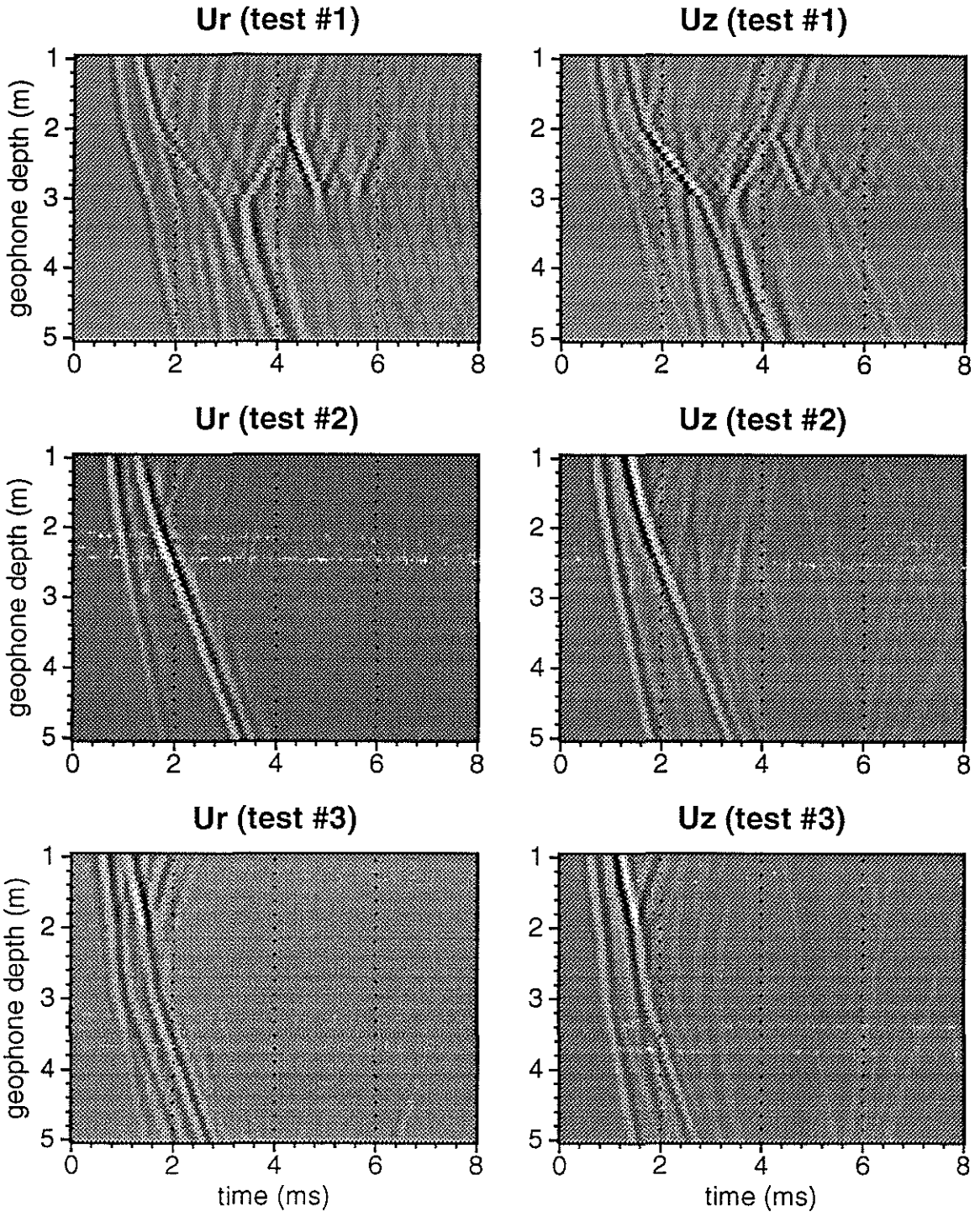

Figure 7: Horizontal and vertical displacements for a volume source in three-layer media with the same first and third layer parameters as in Figure 5. The second layer parameters for the three test cases are tabulated in Table 1.

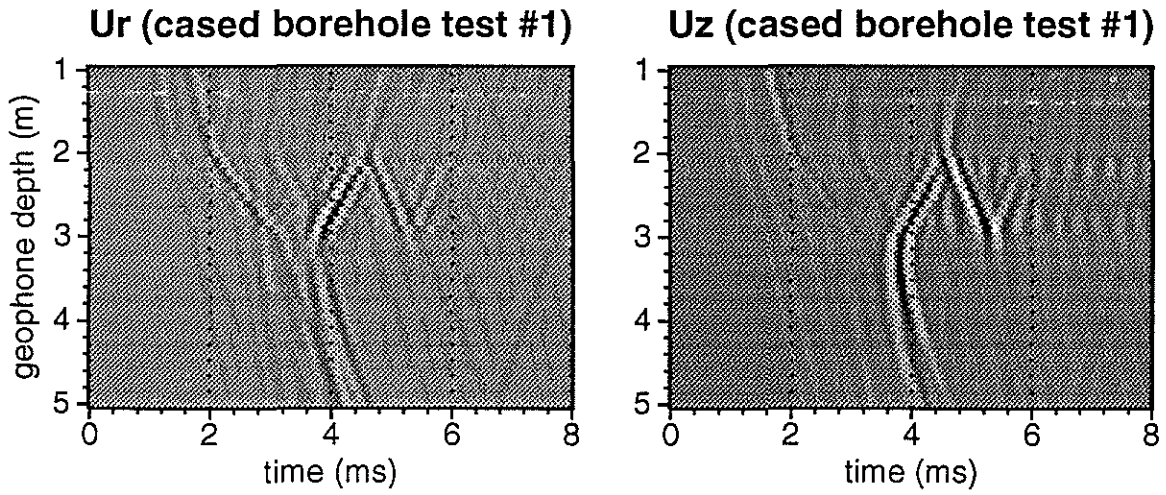

Figure 8: Displacements for an explosion in a cased borehole in the three-layer medium of test #1 in Figure 7. Borehole radius, casing thickness, and cement thickness are 12, 2, 2 in *cm*.